Journal of Zhejiang University-SCIENCE B (Biomedicine & Biotechnology) 2022 23(6):461-480
www.jzus.zju.edu.cn; www.springer.com/journal/11585
E-mail: jzus_b@zju.edu.cn

Research Article

https://doi.org/10.1631/jzus.B2101091

Integrated metabolism and epigenetic modifications in the macrophages of mice in responses to cold stress

Jingjing LU[1*], Shoupeng FU[2*], Jie DAI[3], Jianwen HU[3], Shize LI[1], Hong JI[1], Zhiquan WANG[4], Jiahong YU[1], Jiming BAO[1], Bin XU[1], Jingru GUO[1✉], Huanmin YANG[1✉]

[1]*College of Animal Science and Veterinary Medicine, Heilongjiang Bayi Agricultural University, Daqing 163319, China*
[2]*College of Veterinary Medicine, Jilin University, Changchun 130062, China*
[3]*Shanghai Bioprofile Co. Ltd., Shanghai 201100, China*
[4]*Faculty of Agricultural, Life and Environmental Sciences, University of Alberta, Edmonton, Alberta T5J 4P6, Canada*

Abstract: The negative effects of low temperature can readily induce a variety of diseases. We sought to understand the reasons why cold stress induces disease by studying the mechanisms of fine-tuning in macrophages following cold exposure. We found that cold stress triggers increased macrophage activation accompanied by metabolic reprogramming of aerobic glycolysis. The discovery, by genome-wide RNA sequencing, of defective mitochondria in mice macrophages following cold exposure indicated that mitochondrial defects may contribute to this process. In addition, changes in metabolism drive the differentiation of macrophages by affecting histone modifications. Finally, we showed that histone acetylation and lactylation are modulators of macrophage differentiation following cold exposure. Collectively, metabolism-related epigenetic modifications are essential for the differentiation of macrophages in cold-stressed mice, and the regulation of metabolism may be crucial for alleviating the harm induced by cold stress.

Key words: Low temperature; Stress; Autophagy; Metabolic reprogramming; Histone

1 Introduction

Humans are able to regulate their body temperature very effectively, so temperature stress is often ignored compared to other pathogenic factors such as environment, microbes, and toxic substances. However, low temperature can negatively affect the body's immunity, resulting in increases in the incidence of viral flu, cough, cold, diarrhea, asthma, pneumonia, and other respiratory problems (Budhathoki and Zander, 2019). The number of deaths caused by low temperature in the future is unlikely to decrease, and the resulting health costs may reach one billion euros per year by 2100 (Díaz et al., 2019; Xie et al., 2021). Minimalization of the impact of cold stress should be highly valued. Macrophages are the most functionally diverse innate immune cells, and play an important role in regulating the dynamic immune balance and adaptive immune response. Macrophages differentiate into the M1 pro-inflammatory phenotype by sensing microbial components, such as lipopolysaccharides (LPS), or damage-associated molecular patterns (DAMPs) released from injured tissues. Alternatively, macrophages differentiate into the M2 anti-inflammatory phenotype following stimulation by interleukin-4 (IL-4) or other factors. These forms of macrophage differentiation play key roles in the development of inflammation, disease progression, and tissue and organ repair (Orecchioni et al., 2019; Wang TT et al., 2019). Therefore, to understand the molecular basis of the effect of cold stress on immunity and find an appropriate coping mechanism, we have focused on the effect of cold stress on the differentiation of macrophages.

When exposed to cold, the body needs to generate heat and dissipate energy, which will reshape the

✉ Jingru GUO, guojingru@byau.edu.cn
Huanmin YANG, yanghm@byau.edu.cn
* The two authors contributed equally to this work
Jingru GUO, https://orcid.org/0000-0001-9333-2773
Huanmin YANG, https://orcid.org/0000-0003-3323-6522

Received Dec. 28, 2021; Revision accepted Feb. 14, 2022; Crosschecked May 31, 2022

body's metabolic balance. Macrophage activation is accompanied by metabolic reprogramming, with different metabolic pathways providing energy required for specific forms of immunity (Stienstra et al., 2017; Dumont et al., 2021; Horn and Kielian, 2021). Studies have shown the resting metabolic state of macrophages to be primarily oxidative phosphorylation, ensuring a continuous "scavenger" function (Jha et al., 2015). Differentiation into the M1 inflammatory macrophage phenotype requires cellular commitment to aerobic glycolysis (Warburg effect), which is a simple and fast track to generate adenosine triphosphate (ATP). Aerobic glycolysis satisfies high energy demands required for rapid proliferation, phagocytosis of pathogens, and secretion of pro-inflammatory factors (Fuchs et al., 2019). Thus, the study of immunometabolism can provide new ideas and a better understanding of macrophage differentiation.

Increasing evidence suggests that epigenetic modifications and metabolism are highly interconnected (Saggese et al., 2020; Zheng et al., 2020; Li et al., 2021). Some metabolites (e.g., acetyl-coenzyme A (CoA), α-ketoglutarate, and nicotinamide adenine dinucleotide (NAD^+)) are used as donors or cofactors for epigenetic modifications that regulate gene expression (Hosios and Vander Heiden, 2017; Palzer et al., 2018; Wang ZJ et al., 2018). Importantly, preliminary research in our laboratory demonstrated that cold stress activates microglia by altering the levels of intracellular acetylation that results in a pro-inflammatory condition (Xu et al., 2019). This observation suggests that epigenetic modifications play an important role in regulating immune cell function during cold stress. However, there have been few studies on the mechanisms by which cold stress affects the differentiation of macrophages from the perspective of metabolic-related epigenetic modifications, which hinders our understanding of this biological process.

In this study, we examined the changes in macrophages after cold exposure from a metabolic perspective using multiple omics approaches. We also combined the analysis of metabolism-related epigenetic modification levels to systematically assess the effect of cold stress on the differentiation of mouse macrophages and elucidate the underlying molecular mechanisms.

2 Materials and methods

2.1 Animal experimental models

A total of 160 healthy adolescent male C57BL/6 mice (four weeks old) were purchased from Changsheng Biotechnology Co., Ltd. (Changchun, China). The mice were divided into experimental groups as follows: room temperature (RT) group, cold exposure 1 week (CE1W) group, cold exposure 2 weeks (CE2W) group, and cold exposure 3 weeks (CE3W) group. All experiments were carried out after one week of adaptive feeding. For cold exposure experiments (Xu et al., 2018), between 8:00 a.m. and 8:00 p.m., mice were transferred into a climate chamber at 4 ℃ for 3 h randomly per day, and then back to room temperature. Mice were raised under a room temperature of (24±2) ℃ and 40% relative humidity, under a 12/12-h light/dark cycle, with free access to food and water. All mice were kept in specific pathogen-free conditions prior to use.

2.2 Blood routine examination

After the last cold exposure period, mice were immediately anesthetized. Blood from the retro-orbital plexus was collected into a syringe coated with ethylene diamine tetraacetic acid (EDTA)-lithium and analyzed using a blood routine examination analyzer (IDEXX, USA). For each mouse, a leukocyte count was made.

2.3 Gas exchange analyses

To evaluate the gas exchange levels of mice after cold exposure, mice with similar body weights were monitored using metabolic cages (CLAMS, USA) over 24 h with food ad libitum.

2.4 Primary peritoneal macrophage isolation

Briefly, each mouse was sacrificed after the last cold exposure period. Each mouse was injected intraperitoneally three times with 5 mL of cold phosphate-buffered saline (PBS). Cells were harvested from the abdominal cavity (Ma et al., 2020). The cell suspension was centrifuged at 1300 r/min and then collected into cell culture dishes with RPMI 1640 medium (Gibco, USA) containing 10% (volume fraction) fatal bovine serum (FBS) and 1% (volume fraction) penicillin-streptomycin. Two hours after culture, the floating cells were removed by washing the cells with PBS.

The attached cells were considered peritoneal macrophages (PMs) and were subjected to the experiments. The purity of PMs was confirmed by flow cytometry using cluster of differentiation 11b (CD11b) (BioLegend, USA) and F4/80 (BioLegend) antibodies.

2.5 Quantitative real-time PCR

Total RNA was extracted using TRIzol reagent (Invitrogen, USA), and 5 μg of total RNA was reverse-transcribed using the Transcriptor First Strand cDNA Synthesis Kit (TaKaRa, Japan). Then, quantitative real-time PCR (qPCR) was performed using SYBR Green (TaKaRa) and the following primer pairs: *IL-1β*, 5'-TCG CAG CAG CAC ATC AAC AAG AG-3' (forward) and 5'-TGC TCA TGT CCT CAT CCT GGA AGG-3' (reverse); tumor necrosis factor-α (*TNF-α*), 5'-GCG ACG TGG AAC TGG CAG AAG-3' (forward) and 5'-GCC ACA AGC AGG AAT GAG AAG AGG-3' (reverse); *IL-10*, 5'-TTC TTT CAA ACA AAG GAC CAG C-3' (forward) and 5'-GCA ACC CAA GTA ACC CTT AAA G-3' (reverse); arginase 1 (*Arg1*), 5'-CAG AAG AAT GGA AGA GTC AG-3' (forward) and 5'-CAG ATA TGC AGG GAG TCA CC-3' (reverse); hypoxia-inducible factor-1α (*HIF-1α*), 5'-GAA TGA AGT GCA CCC TAA CAA G-3' (forward) and 5'-GAG GAA TGG GTT CAC AAA TCA G-3' (reverse). Expression levels of target messenger RNAs (mRNAs) were analyzed using the $2^{-\Delta\Delta C_T}$ method and normalized to the expression level of mouse β-actin (Sangon Biotech, China). All fold changes are expressed relative to the control group.

2.6 Quantification of mitochondrial DNA copy number

Total DNA was isolated from the PMs by phenol/chloroform extraction. Mitochondrial DNA (mtDNA) was amplified using primers specific for the mitochondrial cytochrome *c* oxidase subunit 2 (*COX2*) gene, and normalized to genomic DNA by amplification of the ribosomal protein S18 (*Rps18*) nuclear gene. The primers were as follows: *COX2*, 5'-AGT TGA TAA CCG AGT CGT TCT G-3' (forward) and 5'-CTG TTG CTT GAT TTA GTC GGC-3' (reverse); *Rps18*, 5'-TGT GTT AGG GGA CTG GTG GAC A-3' (forward) and 5'-CAT CAC CCA CTT ACC CCC AAA A-3' (reverse).

2.7 Scanning and transmission electron microscopy

PMs were cultured on cell culture slides (SPL Life Sciences, Korea) to observe their surface characteristics. Imaging was performed using an S-520 scanning electron microscope (Hitachi, Japan).

PMs were fixed with 2.5% (volume fraction) glutaraldehyde, dehydrated in ethanol, and embedded in epoxy resin. Then, ultrathin sections (80 nm) of adherent cells were obtained using an ultramicrotome (Leica, Germany). The sections were counterstained with uranyl acetate and lead citrate, and observed using a JEM SX 100 transmission electron microscope (Jeol, Japan) to capture images for evaluation of the integrity of mitochondria by a double-blind method.

2.8 Metabolome analysis

More than 1×10^6 cells were ultrasonically homogenized in 200 μL of chilled water and 800 μL of chilled methanol/acetonitrile (1:1, volume ratio). The samples were centrifuged at 14 000*g* for 20 min at 4 °C and the residue was mixed with 200 μL SDT (4% (volume fraction) sodium dodecyl sulfate (SDS), 100 mmol/L Tris-HCl (pH 7.6), and 100 mmol/L dithiothreitol (DTT) lysis buffer to measure the protein content. L-Glutamate-d5T was added to the supernatant, which was then vacuum-dried and resuspended in 100 μL of 50% (volume fraction) acetonitrile. The samples were centrifuged at 14 000*g* for 15 min at 4 °C and the supernatant was retained for analysis. The intracellular levels of metabolites from the tricarboxylic acid (TCA) cycle pathway, glycolysis pathway, oxidative phosphorylation, and the pentose phosphate pathway (PPP) were determined using liquid chromatography-tandem mass spectrometry (LC-MS/MS). Metabolomic profiling was performed using a Shimadzu Nexera X2 LC-30AD ultrahigh-performance liquid chromatograph (Shimadzu, China) coupled with a QTRAP5500 mass spectrometer (AB SCIEX, USA). The elution solvents consisted of A (acetonitrile:H_2O=5:95, volume ratio) and B (acetonitrile:H_2O=95:5, volume ratio), each containing 10 nmol/L of ammonium bicarbonate (pH 9.0). The elution gradient was set as follows: 95% B (2–9 min), 95% to 70% B (9–10 min), 70% to 30% B (10–11 min), 30% B (11–11.5 min), 30% to 95% B (11.5–15 min), and 95% B. The column temperature was set at 40 °C and the flow rate was 0.3 mL/min. Data were acquired in both electrospray ionization positive and negative modes. The capillary

was 5.5 kV for the positive mode and −4.5 kV for the negative mode. The source temperature was 550 ℃. The data were analyzed using MultiQuant Software (AB SCIEX, USA).

2.9 Glucose consumption

Taking the cell-free group as the control group, after the PMs were cultured in fresh medium for 24 h, the supernatants were collected and glucose concentration was determined by high-performance liquid chromatography (HPLC) using a Sepax Bio-C18 column (4.6 mm×250 mm; Sepax, USA) and a ultraviolet (UV) detector (Agilent, USA) at a wavelength of 192 nm. Glucose consumption (GC) is calculated as the following format: $GC=C_{control}-C_{PM}$, where $C_{control}$ is the glucose concentration in the control group medium, and C_{PM} is the glucose concentration in the PM medium.

2.10 Pyruvate dehydrogenase assay

The pyruvate dehydrogenase (PDH) activity in PMs was measured by a colorimetric method, and analyzed using an assay kit (Solarbio, China) following the manufacturer's protocol.

2.11 Lactate dehydrogenase assay

Lactate dehydrogenase (LDH) activity in PMs was identified by a micromethod, and analyzed using an assay kit (Solarbio) following the manufacturer's instructions.

2.12 Measurement of lactate

The levels of lactate in PMs were quantified by a colorimetric method, and analyzed using an assay kit (Solarbio) following the manufacturer's instructions.

2.13 RNA sequencing of PMs

Total RNA was extracted with a TRIzol-based protocol. An RNA library was constructed using a NEBNext Ultra II RNA Library Prep Kit (NEB, USA). RNA quality was assessed based on the RNA integrity number (RIN), measured using an Agilent 2100 Bioanalyzer (Agilent, USA). Paired-end RNA sequencing (RNA-Seq) was performed using HiSeq 2500 system (Illumina, USA). Sequence reads were aligned to the mouse reference genome (mm10), and gene expression values were calculated from aligned reads using RNA-Seq by expectation maximization (RSEM). Differentially expressed genes (DEGs) were called using edgeR for each experimental design. Functional profiling of DEGs was performed using Gene Ontology (GO) databases.

2.14 Oxygen consumption rate measurements

The oxygen consumption rate (OCR) was measured using a Seahorse XF24 analyzer (Seahorse Bioscience, USA) according to the manufacturer's instructions. Briefly, PMs were plated in an XF24-well microplate (Seahorse Bioscience) and cultured as indicated. The assay medium (extracellular flux base medium containing 1 mmol/L pyruvate, 4 mmol/L glutamine, and 25 mmol/L glucose) was prepared before assay. The OCR was measured in three steps by adding the following reagents: 1.5 μmol/L of oligomycin (Seahorse Bioscience), 2 μmol/L of carbonyl cyanide *p*-trifluoromethoxyphenylhydrazone (FCCP; Seahorse Bioscience), and 0.5 μmol/L of rotenone/antimycin (Seahorse Bioscience). After the measurements were taken, cells were lysed and proteins were quantified using the Enhanced BCA Protein Assay Kit (Beyotime, China).

2.15 Reactive oxygen species assay

Reactive oxygen species (ROS) levels were measured using an ROS Assay kit following the manufacturer's instructions (Beyotime). Briefly, the macrophages were treated with 2',7'-dichlorodihydrofluorescein diacetate (DCFH-DA) solution (10 μmol/L) and then incubated at 37 ℃ for 20 min. After washing the cells with serum-free medium, the cellular fluorescence of ROS production was quantitated by flow cytometry (Beckman, USA) at 488 nm excitation and 525 nm emission wavelengths.

2.16 Autophagic flux assay

To analyze the autophagic flux, pRFP-GFP-hLC3 (Youbio, China) was transfected into PMs by a transient transfection method using Lipo6000™ Tansfection Reagent (Beyotime) following the manufacturer's instructions. The autophagosomes were labeled with yellow dots (a merge of green and red fluorescence), while autolysosomes were labeled with red dots only. After fixation in 4% (volume fraction) paraformaldehyde, a laser scanning confocal microscope (LSCM), the LEICA TCS SP2 (Leica, Germany), was used to analyze the fluorescently labeled light chain 3 (LC3) puncta number.

2.17 Immunofluorescent detection of mitochondria

PMs were seeded on slides and incubated for 24 h at 37 ℃. The cells were then transfected with pEGFP-hLC3 by Lipo6000™ Tansfection Reagent (Beyotime, China). After 24 h, the cells were incubated with a Mito-Tracker Red CMXRos (Beyotime) for 15 min at 37 ℃. Then, 4',6-diamidino-2-phenylindole (DAPI) was used as the nuclear stain, and cells were viewed under a laser scanning confocal microscope (Leica).

2.18 Measurement of mitochondrial membrane potential

JC-1 (Beyotime) can form red fluorescent aggregates in normal mitochondria, but is transformed into green fluorescent monomers in depolarized mitochondria. Here, samples were stained with JC-1 for 20 min at 37 ℃ according to the manufacturer's instructions. The mitochondrial membrane potential ($\Delta\Psi_m$) alternation of cells was viewed under a laser scanning confocal microscope (Leica).

2.19 Total PM protein extraction

Total PM proteins were extracted with 50 μL radio-immunoprecipitation assay (RIPA) buffer (Beyotime) containing 10 mmol/L phenylmethylsulfonyl fluoride (PMSF; Beyotime). Protein concentration was determined using the Enhanced BCA Protein Assay Kit according to the manufacturer's instructions. The samples were stored at −80 ℃ for western blot analysis.

2.20 Mitochondrial isolation and protein extraction

Mitochondria were isolated from PMs, using a Cell Mitochondria Isolation Kit (Beyotime) according to the manufacturer's protocol. Proteins were extracted using mitochondria lysis buffer containing 10 mmol/L PMSF, and protein concentration was determined using the Enhanced BCA Protein Assay Kit according to the manufacturer's instructions.

2.21 Total histone extraction

Total histone was extracted from PMs using the EpiQuik Total Histone Extraction Kit (Epigentek, USA), and the protein concentration was determined using the Enhanced BCA Protein Assay Kit according to the manufacturer's instructions.

2.22 Nuclear protein extraction

Nuclear proteins were extracted from PMs using the Nuclear and Cytoplasmic Protein Extraction Kit (Beyotime), and the protein concentration was determined using the Enhanced BCA Protein Assay Kit, according to the manufacturer's instructions.

2.23 Western blot analysis

About 30 μg of total protein was separated by sodium dodecyl sulfate-polyacrylamide gel electrophoresis (SDS-PAGE) and transferred to a polyvinylidene fluoride (PVDF) membrane (Merck Millipore, USA). Membranes were blocked in 0.05 g/mL nonfat milk in TBST (20 mmol/L Tris-HCl (pH 7.5), 150 mmol/L NaCl, and 0.05% (volume fraction) Tween 20) for 1 h at room temperature, and then incubated overnight at 4 ℃ with the following primary antibodies: HIF-1α (1:1000 (volume ratio, the same below), Cell Signalling Technology, USA), 6-phosphofructo-2-kinase/fructose-2,6-biphosphatase 3 (PFKFB3; 1:1000, Proteintech, China), phosphoglycerate kinase 1 (PGK1; 1:1000, Proteintech), Unc-51-like kinase 1 (ULK1; 1:1000, Proteintech), Beclin1 (1:2000, Proteintech), lysosome-associated membrane protein 2 (LAMP2; 1:1000, Proteintech), p62/sequestosome-1 (SQSTM1; 1:1000, Proteintech), autophagy-related gene 5 (ATG5; 1:1000, Proteintech), LC3 (1:500, Proteintech), dynamin-related protein 1 (Drp1; 1:2000, Proteintech), mitofusin 1 (Mfn1; 1:1000, Proteintech), PTEN-induced kinase 1 (PINK1; 1:1000, Proteintech), Parkin (1:1000, Proteintech), sirtuin 1 (Sirt1; 1:1000, Proteintech), acetylated-lysine (1:1000, Cell Signalling Technology), anti-L-lactyl lysine (1:1000, PTM Bio Inc., China), nuclear factor-κB (NF-κB) p65 (1:1000, Proteintech), phospho-signal transducer and activator of transcription 6 (p-STAT6; 1:1000, Cell Signalling Technology), voltage-dependent anion channel 1/2 (VDAC1/2; 1:1000, Proteintech), lamin B1 (1:5000, Proteintech), histone-H3 (1:3000; Proteintech), and β-actin (1:10000, Proteintech). Membranes were incubated with the appropriate horseradish peroxidase (HRP)-conjugated secondary antibody (1:10000, Proteintech) for 1 h at room temperature. Membranes were then treated with chemiluminescent HRP substrate (Millipore, USA), which was detected using a chemiluminescent imaging system (Bio-Rad, USA). The expression of each protein was measured with Image Lab software (6.0.1).

2.24 Sirt1 activity assay

Sirt1 deacetylase activity was measured using the Sirt1 Assay Kit (Sigma-Aldrich, USA) according to the manufacturer's protocol. Fluorescence intensity was detected at 340 nm excitation and 460 nm emission, and data were acquired through a multifunctional microplate reader (Tecan, Switzerland).

2.25 Dual luciferase assay

PMs were plated in six-well dishes for 12 h and then co-transfected with 2.5 μg pNF-κB-Luc or pSTAT6-Luc and 1 μg pGL4.74[hRluc/TK] vectors (Youbio) using the Lipo6000™ Tansfection Reagent, according to the manufacturer's protocol. After 24 h, the cells were lysed and the luciferase activity was measured using a dual luciferase reporter gene assay kit (Beyotime), according to the manufacturer's instructions. Firefly and Renilla luciferase activity levels were determined, and the relative luciferase activity was normalized to the Renilla luciferase activity.

2.26 Chromatin immunoprecipitation (ChIP)

PMs were treated with fresh 1% (0.01 g/mL) formaldehyde (Cell Signalling Technology) at room temperature to crosslink the proteins bound to the chromatin DNA. Cell lysis, sonication, and immunoprecipitation were performed using the SimpleChIP Enzymatic Chromatin IP Kit (Cell Signalling Technology), according to the manufacturer's instructions. The antibodies for immunoprecipitation were anti-acetylated-lysine (1:100, Cell Signalling Technology), anti-L-lactyl lysine (1:100, PTM Bio Inc.), and IgG (1:100, Cell Signalling Technology). After reverse crosslinking and DNA purification, immunoprecipitated DNA and input DNA were quantified by qPCR using SimpleChIP Universal qPCR Master Mix (Cell Signalling Technology) with primers for histone acetylation and lactylation binding sites in the p65 promoter (forward primer: 5'-CTG TGC CTA CCC GAA ACT CA-3'; reverse primer: 5'-ACT CTG CAG GTG AGA CCA AT-3') and STAT6 promoter (forward primer: 5'-GGT GAG TAA TGG ACT CAG TTG C-3'; reverse primer: 5'-ACA CCT GGG AGG AGG ACT TT-3').

2.27 Statistical analysis

All statistical parameters were calculated using GraphPad Prism 8 software (GraphPad, USA) and Excel software (Microsoft, USA). Differences were analyzed using *t*-tests (for two groups) and one-way analysis of variance (ANOVA) with Dunnett's post-hoc test. $P<0.05$ was considered statistically significant. Values are expressed as means±standard error of the mean (SEM).

3 Results

3.1 Effects of cold stress on macrophage differentiation

In the cold stress model (Fig. 1a), the mice exposed to cold for three weeks were identified as the cold stress group (CE3W). Other mice kept at room temperature formed the control group (RT). Because cold exposure increases the body's metabolism to maintain a constant body temperature, the cold-stressed mice were maintained in metabolic cages to monitor gas exchange levels. Compared to the RT group, cold-stressed mice had significantly higher CO_2 production rate and O_2 consumption rate during the light and dark cycles (Figs. 1c–1f). Routine blood tests found that the number of white blood cells in the blood of cold-stressed mice was significantly higher than that of control mice (Fig. 1b). These results demonstrated that cold stress affected their metabolism and caused an inflammatory response.

PMs were used to assess the response of macrophages to cold stress and to evaluate the inflammation induced by cold stress. These cells have a stable function and phenotype (Layoun et al., 2015). After cold stress, mouse PMs were isolated and the purity of the population was confirmed by flow cytometry (Fig. 1g). Scanning electron microscopy showed that cold stress had changed the morphology of the macrophages, with increased size and pseudopodia (Fig. 1h), suggesting a more active state than that of the RT group. We performed qPCR to evaluate the expression of *IL-1β* and *TNF-α* (which are associated with the M1 macrophage phenotype) as well as *IL-10* and *Arg1* (which are associated with the M2 macrophage phenotype) (Yu et al., 2016). Cold stress significantly increased the expression of *IL-1β*, *TNF-α*, *IL-10*, and *Arg1* mRNA (Fig. 1i). Surprisingly, the increase in *IL-10* and *Arg1* was the most dramatic. These data indicated that cold stress induced not only pro-inflammatory differentiation of macrophages, but also anti-inflammatory differentiation.

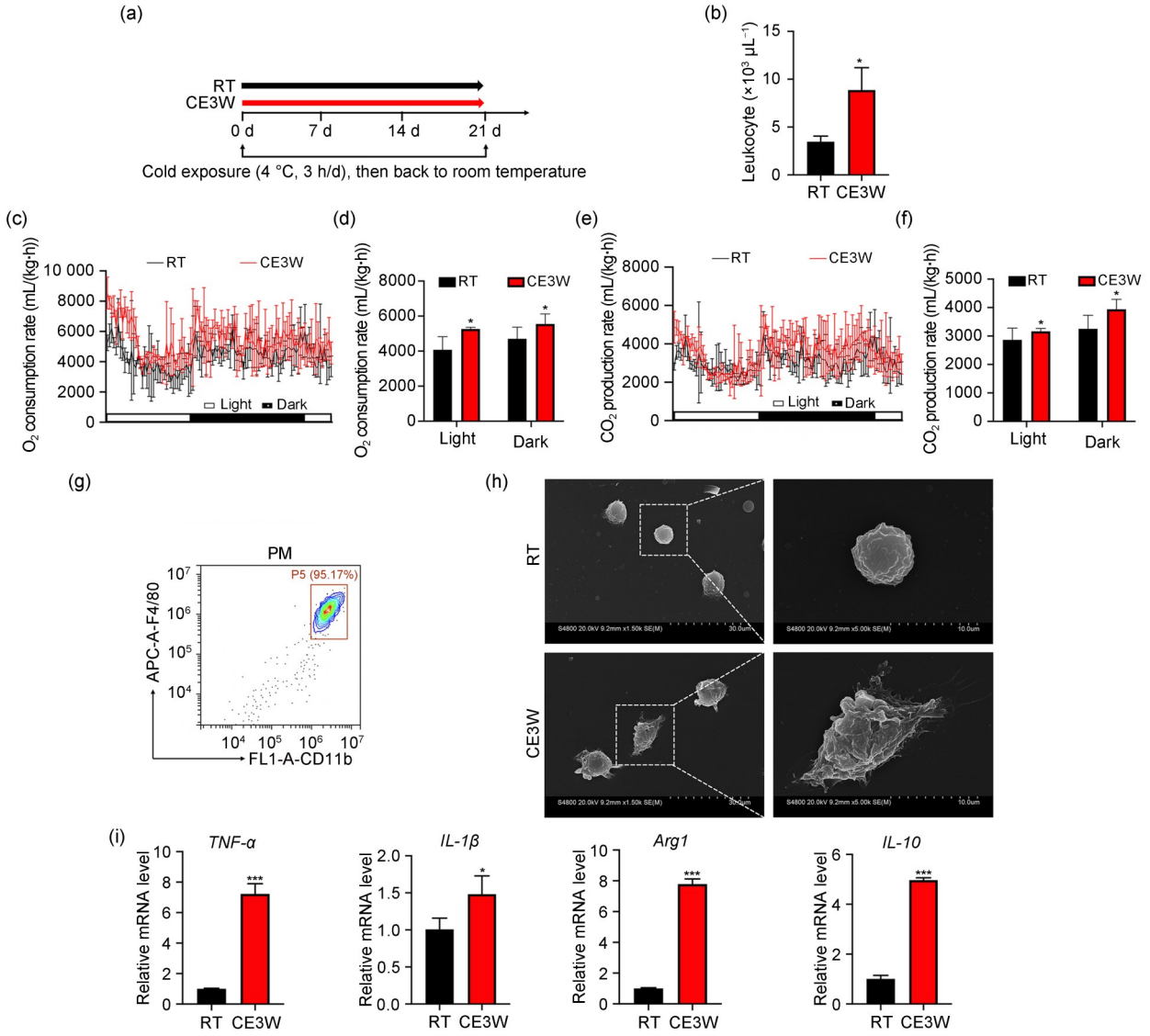

Fig. 1 Induction of inflammation accompanied by increased macrophage activation following cold exposure. (a) The schema of the cold stress model; (b) Leukocyte levels measured in mice following cold exposure (*n*=3 per group); (c, d) The O_2 consumption rates and average O_2 consumption rates of RT and CE3W mice; (e, f) The CO_2 production rates and average CO_2 production rates of RT and CE3W mice; (g) Confirmation of the purity of PMs isolated from RT and CE3W mice by flow cytometry using CD11b and F4/80 antibodies; (h) Representative micrographs of morphological changes in PMs isolated from RT and CE3W mice; (i) Relative mRNA expression of M1-like genes (*TNF-α* and *IL-1β*) and M2-like genes (*Arg1* and *IL-10*) in PMs obtained from RT and CE3W mice (*n*=3 per group). Data represent the mean±SEM. * *P*<0.05, * *P*<0.001, vs. RT. RT: room temperature, the control group; CE3W: cold exposure 3 weeks, the cold stress group; CD11b: cluster of differentiation 11b; *TNF-α*: tumor necrosis factor-α; *IL*: interleukin; *Arg1*: arginase 1; mRNA: messenger RNA; PMs: peritoneal macrophages; SEM: standard error of the mean.**

3.2 Cold stress induces metabolic reprogramming

As the different macrophage phenotypes depend upon differing bioenergy requirements (van den Bossche et al., 2017), we hypothesized that the observed phenotypic changes in PMs might be caused by the effect of cold stress on metabolism. To test this, we performed targeted metabolomic analysis with LC-MS/MS of PMs from control and cold-stressed mice. The metabolites of glycolysis, the TCA cycle, and PPP were measured. We found that with cold stress, metabolites of the glycolytic pathway (pyruvate and lactate) increased significantly. Metabolites of the TCA cycle also changed. α-Ketoglutarate, citrate, and fumarate decreased significantly in the PMs of the CE3W

group, while the levels of malate and oxaloacetate were unchanged (Figs. 2a and 2b). PDH is a key rate limiting enzyme that catalyzes the oxidative decarboxylation of pyruvate in the TCA cycle. To verify the metabolomics results, we analyzed PDH activity using an enzymatic assay. We showed that PDH activity decreased after cold stress (Fig. 2c). In addition, 24-h glucose uptake was assessed by HPLC. The results showed increased glucose uptake in PMs of the CE3W group (Fig. 2d). The expression level of *HIF-1α*, the main transcriptional regulator of glycolysis, was increased significantly (Fig. 2e). These results demonstrated that cold stress induced a metabolic shift to glycolysis in the PMs (Marín Franco et al., 2020).

The time course of cold stress in PMs was assessed at 1, 2, and 3 weeks of cold exposure (Fig. 2f). Results showed that with increasing cold exposure, the protein level of HIF-1α gradually increased (Figs. 2g and 2h). Downstream metabolic enzymes regulated by HIF-1α, such as PFKFB3 and PGK1, are key enzymes driving the glycolytic pathway. Their expression levels gradually increased as well (Figs. 2k and 2l). The activity of LDH, an enzyme that converts pyruvate into lactate, was significantly increased (Fig. 2i). There was an accompanying and gradual increase in the secretion of lactate (Fig. 2j) (Rodríguez-Prados et al., 2010; Yang et al., 2014). These results further confirmed that cold stress induced the activation of glycolytic metabolism in the macrophages. Overall, these data support the conclusion that the differentiation of macrophages induced by cold stress may be shaped by the metabolic reprogramming of glycolysis.

3.3 Whole-genome sequencing of PMs

We performed RNA-seq analysis to further understand how macrophage phenotypes are regulated by associated metabolic patterns. To examine how PMs respond to cold stress, we performed genome-wide RNA-seq on freshly isolated PMs from control and cold-stressed mice. Compared with the RT group, changes in gene expression were detected in the PMs of the CE3W group, including 158 up-regulated and 173 down-regulated genes (Fig. 3a). GO analysis showed that "response to stress," corresponding to genes related to body stress injury or stress response recovery, was the most significantly enriched biological process (2.31×10^{17}) caused by cold stress. The top 20 significantly ($P<0.05$) enriched biological processes of DEGs were related to the immune system, organic metabolism, inflammation, and cell migration (Fig. 3b). Examples included "immune system process," "response to organic substance," "response to cytokine," and "regulation of cell migration." These results suggested that cold stress interfered with immune metabolism, the inflammatory response, and the function of macrophages. Next, we compared the first 15 biological processes that were significantly enriched in PMs (up-regulated genes and down-regulated genes) of the CE3W group. The up-regulated genes were mostly related to inflammatory factors and the immune system, while the down-regulated genes were mostly related to cell migration (Figs. 3c and 3d). In general, these results indicate that cold stress activates the immune response of macrophages, induces inflammation, and inhibits the movement of macrophages.

3.4 Cold stress damages macrophage mitochondria

As the center of energy metabolism, the dynamic network of mitochondrial fusion and fission is essential for adaptation to the energy needs of cells in different environments (Lu, 2009). Since the down-regulated genes of PMs of the CE3W group were significantly enriched in biological process related to "cell dynamics," we hypothesized that this may be due to the disruption of mitochondrial homeostasis. To test this, we assessed the expression of the main mitochondrial fission protein Drp1 and the main mitochondrial fusion protein Mfn1 by western blot. Results showed that cold stress significantly increased the expression of Drp1 and decreased the expression of Mfn1 (Figs. 4a and 4b). qPCR results also showed a deletion of mtDNA (Fig. 4c). Note that in previous studies, the change in this process usually occurred in inflammatory immune cells (such as macrophages) related to the destruction of the electron transport chain (ETC) (Katoh et al., 2017). Damage to the ETC increases the flow of leaking electrons, decreases $\Delta\Psi_m$, and increases ROS (Kalghatgi et al., 2013). Consistent with those observations, the production of ROS and the loss of $\Delta\Psi_m$ were increased by cold stress (Figs. 4d and 4g). We also measured the OCR after addition of oligomycin (an ATP synthase inhibitor), the FCCP (H^+ ionophore), as well as rotenone and antimycin A (ETC inhibitors) in real time to detect mitochondrial function. Compared with the RT group, maximum respiratory capacity was reduced in PM mitochondria of the CE3W group (Fig. 4e).

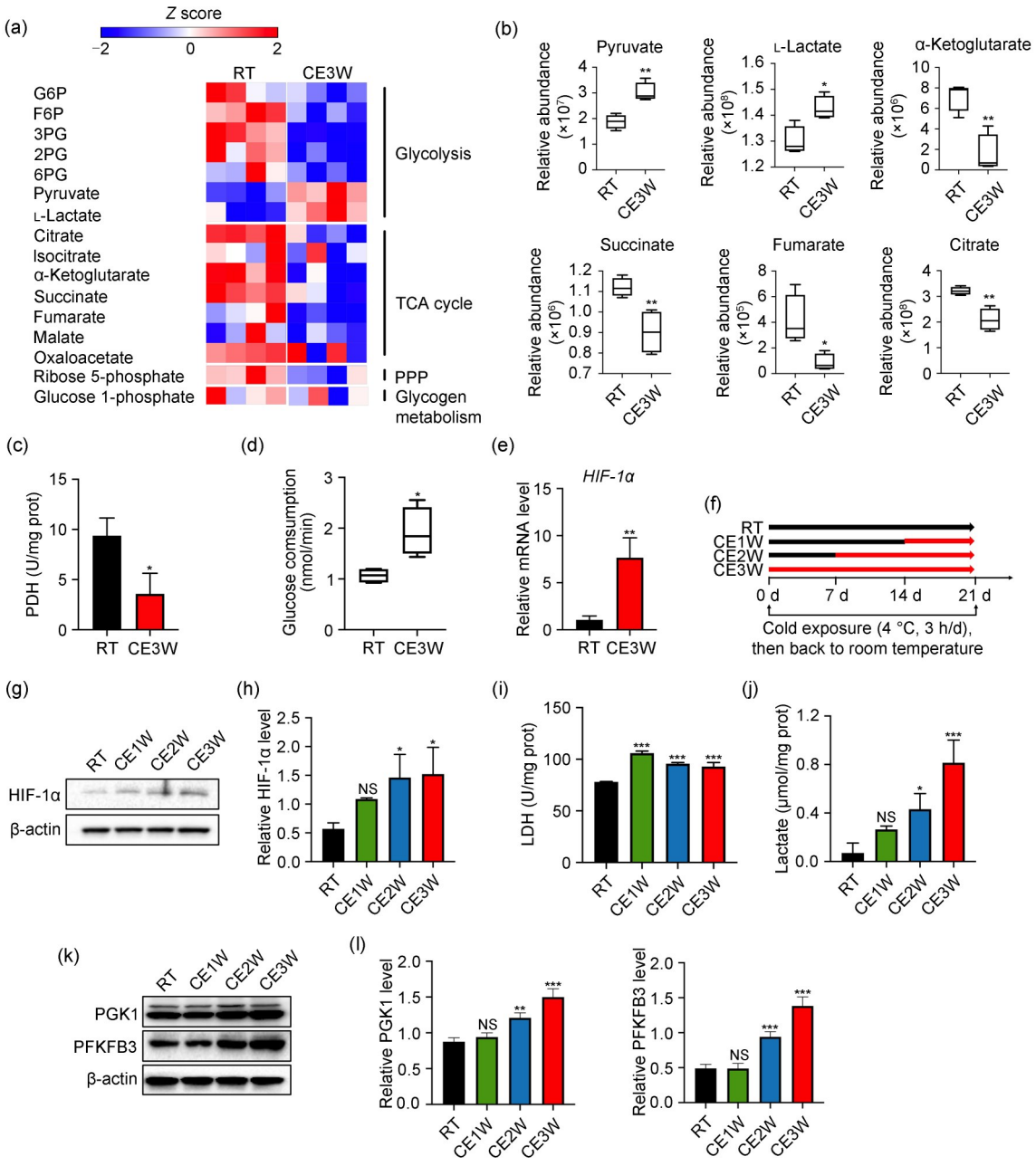

Fig. 2 Metabolic reprogramming underlies PM differentiation following cold exposure. (a) Heatmap of energy metabolism levels, as measured by targeted metabolomics in PMs obtained from RT and CE3W mice (*n*=4 per group); (b) Graphs for selected metabolites from panel (a); (c, d, e) PDH activity, relative glucose consumption, and relative mRNA expression of *HIF-1α* in PMs obtained from RT and CE3W mice (*n*=3 per group); (f) The schema of isolation of PMs from RT, CE1W, CE2W, and CE3W mice; (g, h) Western blot analysis of protein levels of HIF-1α in PMs obtained from RT, CE1W, CE2W, and CE3W mice (*n*=3 per group); (i, j) Measurement of LDH activity and intracellular lactate levels in PMs obtained from RT, CE1W, CE2W, and CE3W mice (*n*=3 per group); (k, l) Western blot analysis of protein levels of PGK1 and PFKFB3 in PMs obtained from RT, CE1W, CE2W, and CE3W mice (*n*=3 per group). Data represent the mean±SEM. NS (not significant), * *P*<0.05, ** *P*<0.01, * *P*<0.001, compared to RT, using one-way ANOVA with Dunnett's post-hoc test. RT: room temperature, the control group; CE1W: cold exposure 1 week, the cold stress group; CE2W: cold exposure 2 weeks, the cold stress group; CE3W: cold exposure 3 weeks, the cold stress group; G6P: glucose 6-phosphate; F6P: fructose 6-phosphate; 3PG: 3-phosphoglycerate; 2PG: 2-phosphoglycerate; 6PG: 6-phosphoglycerate; TCA: tricarboxylic acid; PPP: pentose phosphate pathway; PDH: pyruvate dehydrogenase; HIF-1α: hypoxia-inducible factor-1α; mRNA: messenger RNA; LDH: lactate dehydrogenase; PGK1: phosphoglycerate kinase 1; PFKFB3: 6-phosphofructo-2-kinase/fructose-2,6-biphosphatase 3; PM: peritoneal macrophage; SEM: standard error of the mean; ANOVA: analysis of variance.**

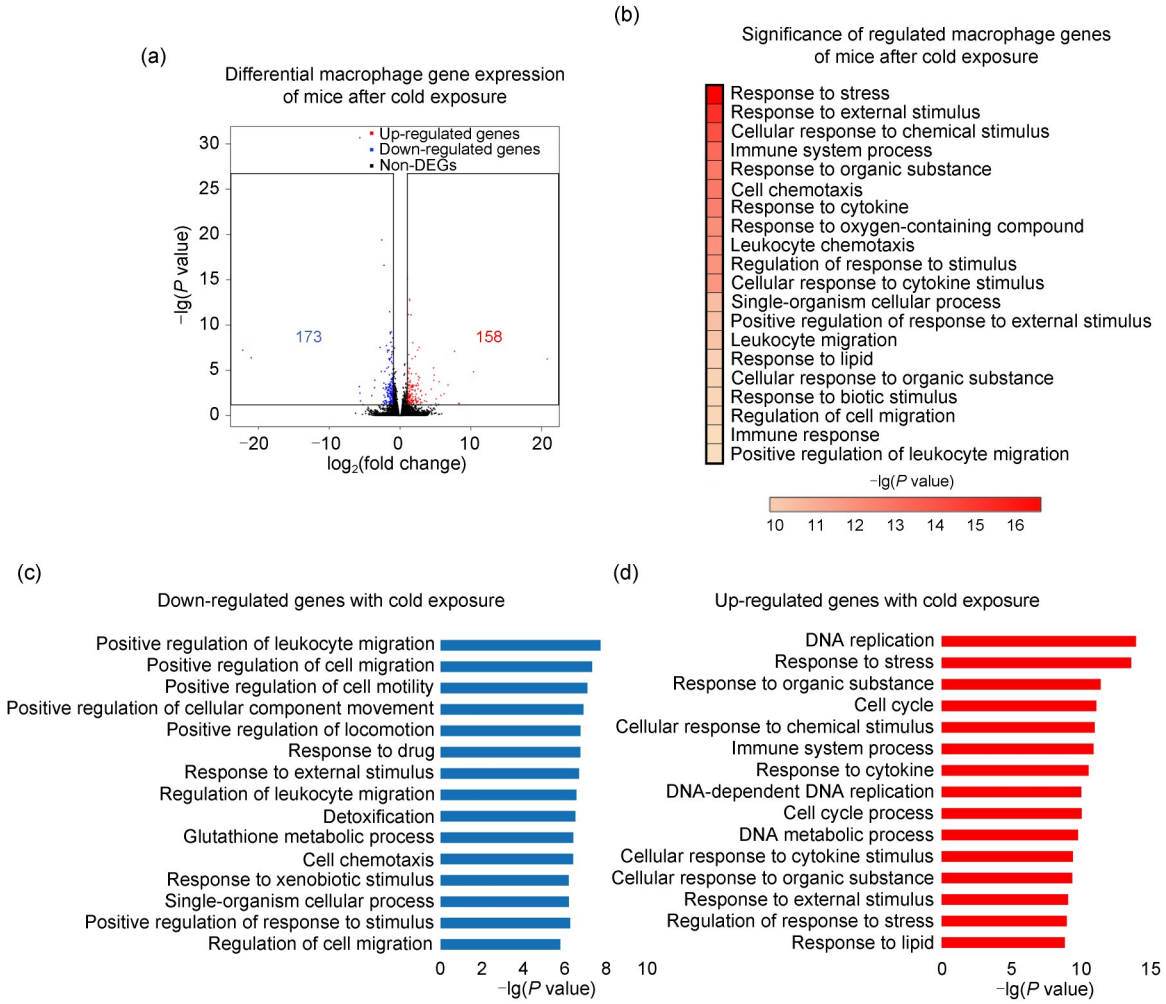

Fig. 3 Gene expression in isolated PMs from RT mice and CE3W mice. (a) A volcano plot of differential PM gene expression of mice after cold exposure; (b) The top 20 significantly (P<0.05) enriched BPs among differentially expressed genes, with the significance of BPs being indicated by the intensity of red color; (c) The top 15 significantly (P<0.05) enriched-BPs among genes down-regulated after cold exposure; (d) The top 15 significantly (P<0.05) enriched BPs among genes up-regulated after cold exposure. PM: peritoneal macrophage; RT: room temperature, the control group; CE3W: cold exposure 3 weeks, the cold stress group; BP: biological process; DEG: differentially expressed gene (Note: for interpretation of the references to color in this figure legend, the reader is referred to the web version of this article).

Mitophagy is a process by which cells clear damaged mitochondria, ensuring the integrity of the mitochondrial network. To determine whether cold stress induced mitophagy in macrophages, we evaluated the expression of mitochondrial LC3, which is an indicator of autophagosome formation. PMs were transfected with the GFP-LC3 plasmid, and mitochondria were labeled with Mito-Tracker Red. Mitophagy was marked as a yellow dot (combination of green and red fluorescence) and investigated by confocal microscopy. The results showed that cold stress promoted the accumulation of mitochondrial LC3 in macrophages (Fig. 4f). Further, the mitophagy-related proteins, PINK1 and Parkin (Yu et al., 2020), showed a similar expression trend after cold exposure (Figs. 4i and 4j). Transmission electron microscopy (TEM) examination showed that the number of autophagosome double-membrane vesicles was increased in the PMs of cold-stressed mice (Fig. 4h), which is consistent with the results of western blots and confocal microscopy.

3.5 Cold stress increases macrophage autophagy

With stress, autophagy promotes cell survival by eliminating damaged cell components, and maintaining nutrient and energy homeostasis (Sun et al., 2013). PMs were transfected with the RFP-GFP-LC3 plasmid.

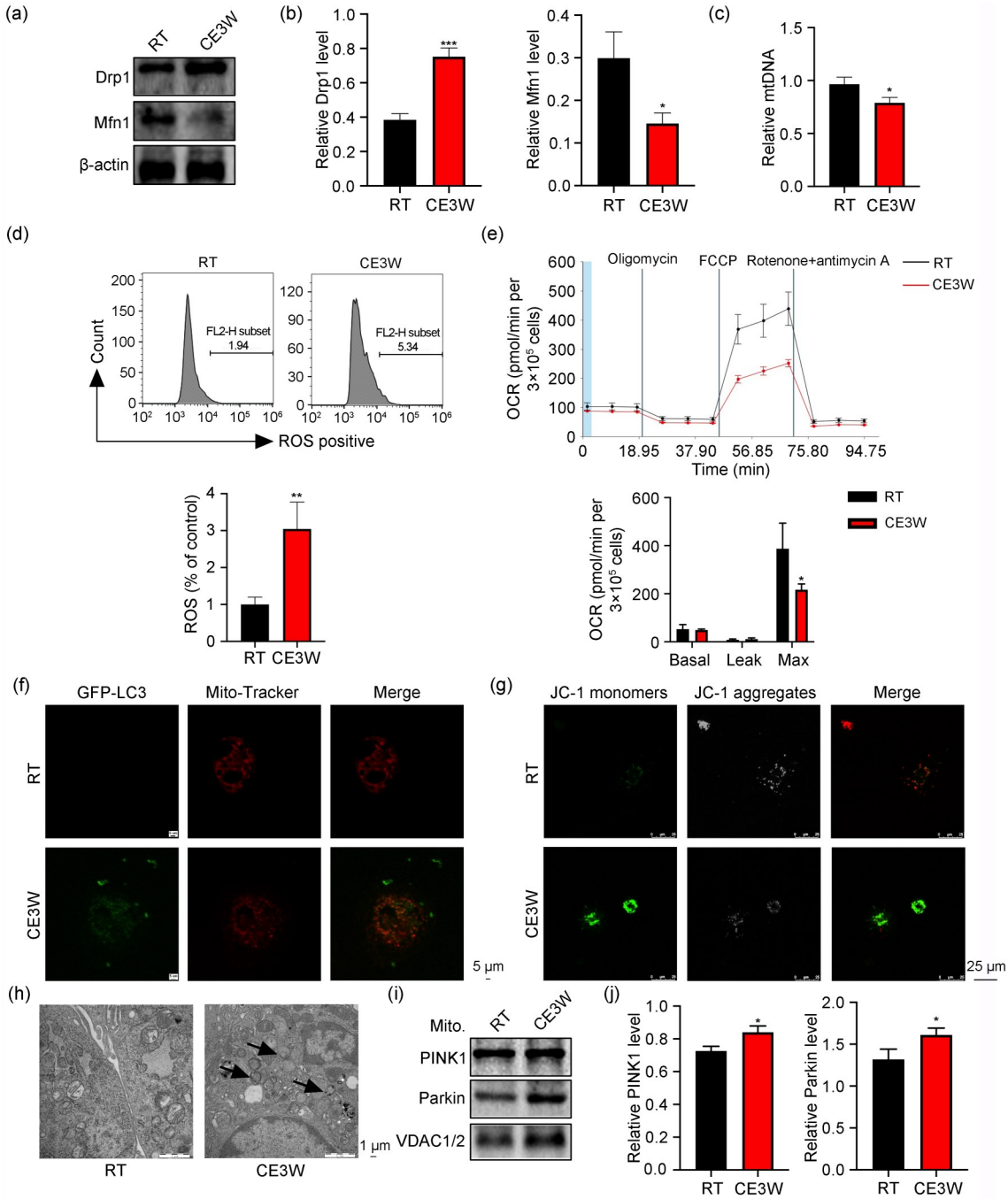

Fig. 4 Mitochondrial dysfunction and increased mitochondrial autophagy in PMs following cold exposure. (a, b) Western blot analysis of protein levels of Drp1 and Mfn1 in PMs obtained from RT and CE3W mice (*n*=3 per group); (c) The relative mtDNA content measured by qPCR in PMs obtained from RT and CE3W mice (*n*=3 per group); (d) The levels of ROS in PMs of RT and CE3W mice measured by flow cytometry (*n*=3 per group); (e) The OCR in PMs obtained from RT and CE3W mice (*n*=4 per group); (f) Mitophagy determined by measuring the LC3 located in mitochondria, scale bar= 5 μm; (g) Measurement of $\Delta\psi_m$ (the color change is due to contrast issues), scale bar=25 μm; (h) Measurement of mitochondrial changes, scale bar=1 μm; (i, j) The mitochondrial (Mito.) protein levels of PINK1 and Parkin in PMs of RT and CE3W mice (*n*=3 per group). Data represent the mean±SEM. * *P*<0.05, ** *P*<0.01, *** *P*<0.001, vs. RT. PM: peritoneal macrophage; Drp1: dynamin-related protein 1; Mfn1: mitofusin 1; RT: room temperature, the control group; CE3W: cold exposure 3 weeks, the cold stress group; mtDNA: mitochondrial DNA; ROS: reactive oxygen species; OCR: oxygen consumption rate; FCCP: *p*-trifluoromethoxyphenylhydrazone; $\Delta\psi_m$: mitochondrial membrane potential; GFP: green fluorescent protein; LC3: light chain 3; PINK1: PTEN-induced kinase 1; VDAC1/2: voltage-dependent anion channel 1/2; qPCR: quantitative real-time polymerase chain reaction; SEM: standard error of the mean.

Autophagosomes were marked as yellow dots, and autophagolysosomes as red dots. Confocal microscopy showed that the number of yellow and red dots in the PMs of cold-stressed mice increased in parallel when compared with the control (Fig. 5a), indicating that cold stress increased the autophagy flux of PMs. Next, we studied changes in autophagy during cold stress. With cold stress we assessed ULK1 (autophagy initiation factor), Beclin1 and ATG5 (two autophagy-related proteins necessary for the formation of autophagosomes), isoform conversion of LC3 (an indicator of autophagosome formation), p62/SQSTM1 (ubiquitin-binding scaffold protein selectively degraded by autophagy), and LAMP2 (Huang et al., 2018). According to western blot analysis, ULK1, Beclin1, ATG5, LC3 II/I, and LAMP2 gradually increased with cold exposure (Figs. 5b and 5c), indicating an increase in autophagosomes and lysosomes, consistent with the

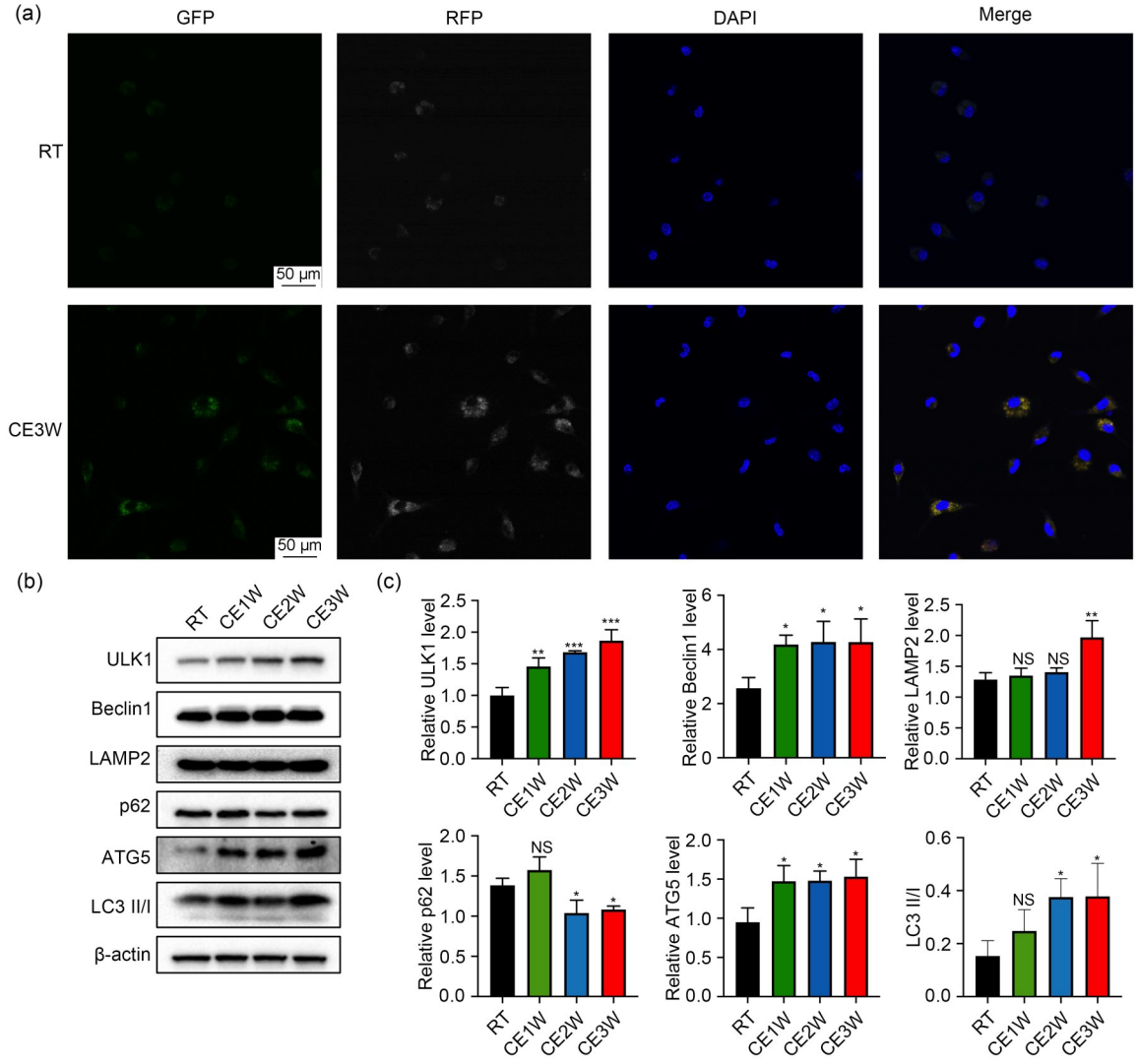

Fig. 5 Enhanced autophagy in PMs following cold exposure. (a) The LSCM imaging of autophagic flux in PMs of RT and CE3W mice (the color change is due to contrast issues); (b, c) Western blot analysis of protein levels of ULK1, Beclin1, LAMP2, p62, ATG5, and LC3 II/I in PMs obtained from RT, CE1W, CE2W, and CE3W mice (n=3 per group). Data represent the mean±SEM. NS (not significant), $^{*}P$<0.05, $^{**}P$<0.01, $^{***}P$<0.001, vs. RT, using one-way ANOVA with Dunnett's post-hoc test. PM: peritoneal macrophage; LSCM: laser scanning confocal microscope; RT: room temperature, the control group; CE1W: cold exposure 1 week, the cold stress group; CE2W: cold exposure 2 weeks, the cold stress group; CE3W: cold exposure 3 weeks, the cold stress group; GFP: green fluorescent protein; RFP: red fluorescent protein; DAPI: 4', 6-diamidino-2-phenylindole; ULK1: Unc-51-like kinase 1; LAMP2: lysosome-associated membrane protein 2; ATG5: autophagy-related gene 5; LC3: light chain 3; SEM: standard error of the mean; ANOVA: analysis of variance.

autophagy flux results. Note that the initial increase and then decrease in p62 levels may have been due to excessive degradation.

3.6 Histone acetylation and lactylation regulate macrophage differentiation

Sirtuins are deacetylases found throughout the body, and Sirt1 is one of the most prominent (Kang et al., 2020). We found that cold stress significantly reduced the enzyme activity of Sirt1 (Fig. 6a). As exposure to cold increased, protein levels of Sirt1 also gradually decreased (Figs. 6b and 6c). There is increasing evidence that metabolic pathways influence the regulation of epigenetic genes by providing donors and cofactors for epigenetic modification (van Winkle and Ryznar, 2019; Wang ZQ et al., 2019). A recently discovered histone modification, histone lactylation, uses lactate as a modification donor to regulate gene expression (Zhang et al., 2019). Building on earlier findings in our laboratory, we used western blotting to evaluate whether the accumulation of lactate induced by cold stress-mediated glycolytic metabolism reprogramming is involved in changing the epigenetic status of PMs. The results showed that cold stress increased levels of both histone acetylation and lactylation. A gradual increase in histone lactylation was associated with an increase in cold exposure (Figs. 6d and 6e). Next, we assessed the impact of cold stress-induced epigenetic modifications on the differentiation of macrophages. ChIP was used to examine acetylation and lactylation of histone in the promoter regions (2000 bp before the transcription start site) of NF-κB (p65) (M1 macrophage core transcription factor) and STAT6 (M2 macrophage core transcription factor) (Chen et al., 2017). The results showed that cold exposure increased histone acetylation in the promoter of NF-κB (p65) promoter, while histone lactylation was more significantly elevated in the promoter of STAT6 (Fig. 6f). The dual luciferase reporter gene was used to assess promoter activity, and nuclear protein separation was used to assess nuclear entry of transcription factors. Cold stress increased promoter activity for NF-κB (p65) and STAT6 (Fig. 6g) as well as nuclear translocation (Figs. 6h and 6i). Taken together, these results demonstrate that cold stress induces macrophage M1 pro-inflammatory differentiation and M2 anti-inflammatory differentiation, which correlates with increased levels of the histone acetylation and lactylation.

4 Discussion

Cold exposure can result in inflammation as well as an increased susceptibility to various diseases, including the common cold. The correct functional response of macrophages to microenvironmental stimuli and signals plays an important role in host protection (Delavary et al., 2011). We found that mitochondrial dysfunction induced by cold stress might be an important causative factor that mediates the pro-inflammatory differentiation of macrophages, resulting in inflammation. Based on the observed experimental results, we speculated that abnormal mitochondrial function promotes metabolic reprogramming of macrophage aerobic glycolysis, inducing macrophage M1 pro-inflammatory differentiation and the release of inflammatory factors. In turn, the aerobic glycolytic metabolism of M1 macrophages leads to the accumulation of lactate. Macrophages then undergo histone lactylation, which initiates repair gene expression. We provided evidence that histone acetylation and lactylation synergistically participate in the response of macrophages to cold stress, promoting the differentiation of M1 and M2 macrophages. With the accumulation of lactate, the expression of anti-inflammatory (M2) genes gradually increased. This may be a self-protective mechanism by which mitochondrial function and metabolically related epigenetic modifications regulate inflammation caused by cold stress.

Based on previous research at this laboratory, adolescent mice with a high degree of sensitivity to cold stress were selected for assessment. Following cold exposure for three weeks, O_2 absorption volume and CO_2 release volume increased, suggesting that whole-body high-energy expenditure is required to resist the adverse effects of cold stress. The white blood cell count also increased, indicating inflammation induced by cold stress (Xu et al., 2021). Effective nutrient distribution between tissues and cells is a basic characteristic of multicellular organisms. Whole-body high-energy mobilization is bound to cause changes within cellular microenvironments (McMurtrey, 2016). Macrophages are innate immune cells that reside in most tissues of the body. Their immune barrier and

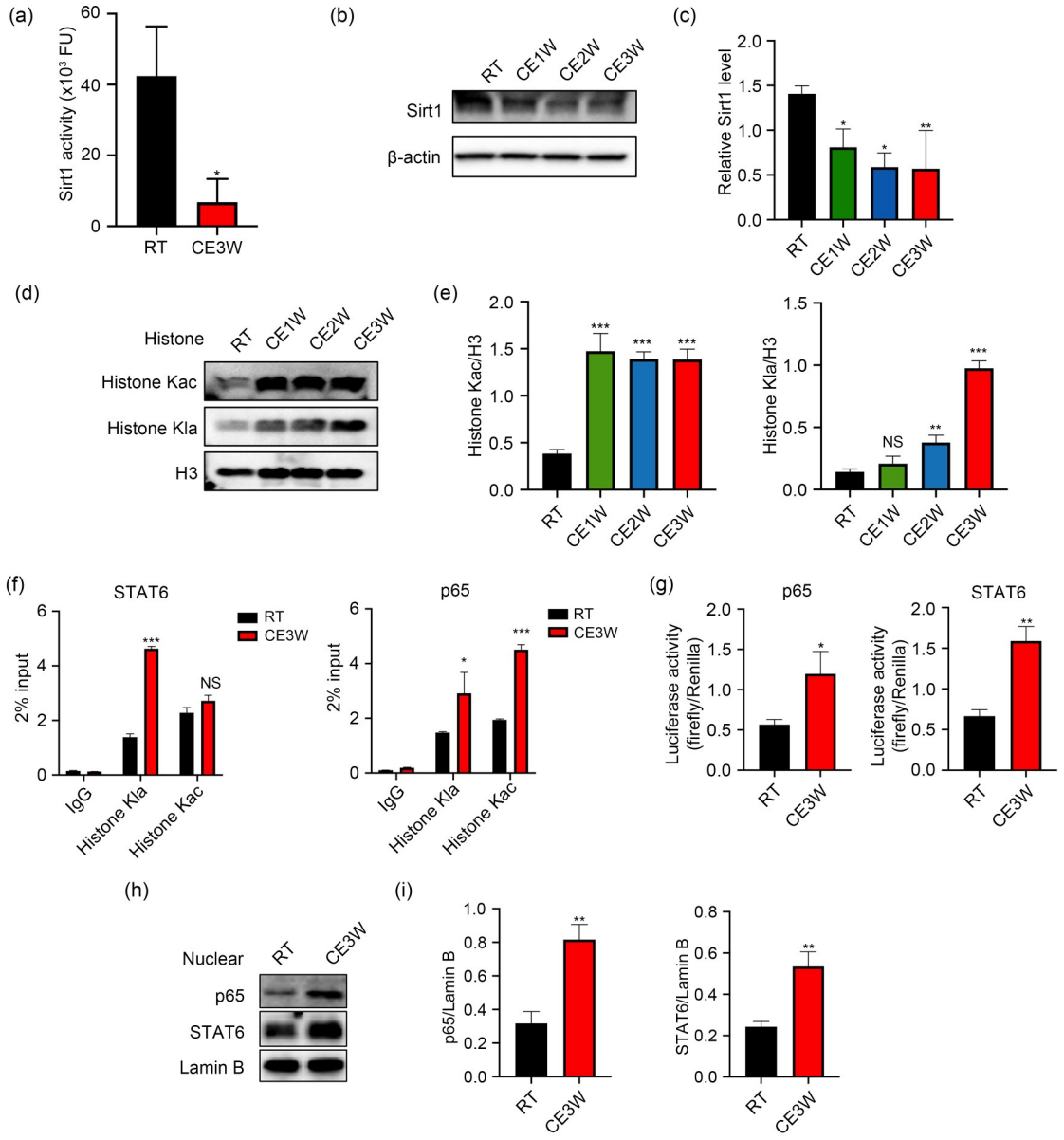

Fig. 6 Macrophage differentiation induced by cold stress via histone acetylation and lactylation. (a) Activity analysis of Sirt1 in PMs obtained from RT and CE3W mice (*n*=3 per group); (b, c) Western blot analysis of protein levels of Sirt1 in PMs obtained from RT, CE1W, CE2W, and CE3W mice (*n*=3 per group); (d, e) Western blot analysis of histone acetylation and lactylation in PMs obtained from RT, CE1W, CE2W, and CE3W mice (*n*=3 per group); (f) Histone acetylation and lactylation occupancy analysis by ChIP-qPCR in PMs obtained from RT and CE3W mice (*n*=3 per group); (g) p65 and STAT6 promoter activity measured by luciferase reporter gene assay in PMs of RT and CE3W mice (*n*=3 per group); (h, i) Western blot analysis of relevant nucleoprotein expression levels of p65 and STAT6 in PMs obtained from RT and CE3W mice (*n*=3 per group). Data represent the mean±SEM, using one-way ANOVA with Dunnett's post-hoc test. NS (not significant), $^{*}P<0.05$, $^{**}P<0.01$, $^{***}P<0.001$, vs. RT. Sirt1: sirtuin 1; PM: peritoneal macrophage; RT: room temperature, the control group; CE1W: cold exposure 1 week, the cold stress group; CE2W: cold exposure 2 weeks, the cold stress group; CE3W: cold exposure 3 weeks, the cold stress group; Kac: acetylation; Kla: lactylation; H3: histone 3; STAT6: signal transducer and activator of transcription 6; ChIP: chromatin immunoprecipitation; qPCR: quantitative real-time polymerase chain reaction; SEM: standard error of the mean; ANOVA: analysis of variance.

surveillance functions ensure their leading role in maintaining homeostasis in response to adverse stimuli (Kaur et al., 2017). Thus, from the perspective of immunometabolism, we analyzed the impact

of cold stress on macrophages. We found that cold stress induced macrophage activation. The response of macrophages to cold stress was accompanied by simultaneous up-regulation of M1-like genes (*IL-1β* and *TNF-α*) and M2-like genes (*IL-10* and *Arg1*). That is, bidirectional differentiation occurred.

With their high degree of plasticity, macrophages play diverse roles in tissue homeostasis and the adaptive immune response (Iavarone et al., 2020). The strict control of energy metabolism serves as the basis for macrophage reactive phenotypes (di Conza and Ho, 2018). Thus, we first analyzed energy metabolism in the PMs of the cold stress mouse model. Results suggested that cold stress promoted metabolic reprogramming of aerobic glycolysis, which was the metabolic state of the M1 macrophages. These metabolic changes were accompanied by accumulation of lactate and suppression of the TCA cycle. In previous reports, complex changes in cell metabolism were found to be due to HIF-1α activation that resulted in glucose uptake and overall enhanced glycolysis (Malhotra et al., 2002; Codo et al., 2020), and inhibition of PDH activity, which reduces aerobic oxidation of glucose in mitochondria (Mathew and White, 2011). Consistent with those reports, chronic cold stress gradually increased the expression of macrophage HIF-1α and key glycolytic enzymes (PGK1 and PFKFB3), as well as LDH activity. These results demonstrated HIF-1α involvement in regulation of the glycolytic metabolic reprogramming of macrophages induced by cold stress, even with sufficient oxygen. The stabilization of HIF-1α requires the induction of hypoxic conditions, which excludes nonhypoxic HIF-1α stabilization by fumaric and succinic acid reductions due to glucose metabolism (Schito and Rey, 2018). On the other hand, cellular metabolic processes located in the mitochondria, such as the TCA cycle, were generally defective in the PMs of cold-stressed mice. These results imply that cold stress may cause mitochondrial damage, affecting the perception of intracellular oxygen with resultant reprogramming of glycolysis metabolism. This reprogramming would promote pro-inflammatory (M1) macrophage differentiation and the inflammatory phenotype. However, increased expression of anti-inflammatory genes was also observed. This is in contrast to the previous understanding that aerobic glycolysis was the core metabolic mode for M1 macrophages, a metabolic mode expected to promote an inflammatory macrophage response (Wang FL et al., 2018).

A comparison of gene expression in PMs from cold-stressed mice and control mice showed that cold stress causes mitochondrial function defects in PMs. Mitochondrial function is determined by a number of factors including their mass, density, and distribution. The state of mitochondrial fusion and fission reflects mitochondrial mass. The network of fusion is more conducive to the use of glucose for energy needs, while fission isolates mitochondria from harmful substances to avoid more damage (Youle and van der Bliek, 2012). When the body is subjected to stimuli, it will reshape mitochondria to cope with the needs of energy intensive biological processes (MacVicar et al., 2019). With cold stress, macrophages expressed high levels of Drp1 and reduced levels of Mfn1, suggesting that mitochondrial homeostasis had been destroyed. Mitochondrial fusion plays an important role in ensuring the accuracy and stability of mtDNA replication, and a reduction of Mfn1 leads to mtDNA deletion (Suárez-Rivero et al., 2017). Furthermore, increased fission usually induces defects in the mitochondrial ETC, which leads to an increase in production of ROS and reduces mitochondrial respiratory capacity (Indo et al., 2007; Zheng et al., 2021). These results may force PMs to use bioenergy replacement mechanisms such as glycolysis. In addition, cold stress may increase the degree of proton leakage mediated by uncoupling proteins located in the inner membrane of mitochondria (Shang et al., 2009). The conversion of more metabolic energy into heat to be emitted to maintain a constant body temperature under cold conditions reduces the $\Delta\Psi_m$ and aggravates mitochondrial damage. Importantly, excessive fission also induces the miniaturization of mitochondria, which cannot be repaired by fission, when the mitochondria are damaged. Mitophagy is the targeted phagocytosis and destruction of mitochondria by autophagosomes, and is generally considered to be the main mechanism for mitochondrial quality control (Hoshino et al., 2019). However, abnormal mitochondrial autophagy would aggravate cell damage (Kang et al., 2021). In our study, we observed that cold stress activated mitochondrial autophagy in PMs, as shown by the increased expression of PINK1 and Parkin proteins, high colocalization of LC3 on mitochondria, and accumulation of mitophagosomes. These data imply

that damage to the mitochondrial function of PMs caused by cold stress is a potential factor leading to aerobic glycolysis.

To increase adaptability to a cold environment, continuous high-level energy mobilization is needed to maintain normal body function. Despite continuous dietary intake, prolonged stress would increase the functional burden, forcing macrophage adaptation to the change in the microenvironment. In the case of undernutrition, autophagy is a homeostatic process, which promotes the circulation of cellular components through a "decomposition and reuse" model, thereby maintaining macromolecular metabolites such as proteins, nucleotides, fatty acids, and membrane lipids. Autophagy compensates for a lack of substrates for energy generation and biosynthetic pathways by degrading macromolecules (Castillo et al., 2013; Matus et al., 2014). Consistent with this, cold exposure increased macrophage autophagy, as demonstrated by the gradual increase in expression of autophagy-related proteins, such as ULK1, ATG5, Beclin1, and LC3 II/I. Further, a gradual increase in the formation of phagolysosomes was observed. This may have been due to the degradation of macromolecules required to meet the metabolic needs of macrophages undergoing differentiation in response to cold stress. However, excessive autophagy would destroy macrophage structure and disrupt normal immunological function.

Recent developments in the field of immunometabolism have revealed that metabolites regulate a variety of transcriptional responses, including epigenetic modification (Amiel and Perona-Wright, 2020; Lio and Huang, 2020). These developments suggest that metabolism goes beyond its traditional roles in bioenergetics and biosynthesis. The main metabolite of glycolysis, lactate, is no longer considered "metabolic waste." The lactate-derived lactylation of histone lysine residues is an epigenetic modification, which initiates the transcription of anti-inflammatory genes in response to metabolic reprogramming following a macrophage inflammatory response. Consistent with previous laboratory results (Xu et al., 2018), cold exposure increased histone acetylation, while enzymatic activity and protein expression of Sirt1, a key deacetylase, gradually decreased. With an increase in glycolysis, the accumulation of lactate in macrophages would result in histone lactylation, which in conjunction with histone acetylation would affect the differentiation of macrophages through modification of NF-κB (p65) and STAT6 promoters. Generally, histone acetylation is related to inflammation mediated by macrophages (Hardbower et al., 2017; Singh et al., 2018). In contrast, histone lactylation promotes M2 anti-inflammatory differentiation, reducing excessive inflammation. Therefore, we speculate that the differentiation of macrophages during cold stress may be the result of multilayered epigenetics, regulated by histone acetylation and lactylation. We propose such a biological process. As such, cold stress-induced metabolic reprogramming of macrophage aerobic glycolysis would destroy the integrity of mitochondrial function, which in conjunction with increased histone acetylation would promote pro-inflammatory differentiation of M1 macrophages. With the accumulation of intracellular lactate driven by glycolysis, histone lactylation would initiate the transcription of STAT6, upregulating the expression of repair genes and the body's self-protective mechanisms (Fig. 7). However, when the inflammatory stimulus persists and cannot be destroyed, the abnormally prolonged or excessive inflammatory response will lead to tissue damage and chronic inflammation.

In summary, our results demonstrate that metabolic reprogramming, which induces differentiation of macrophages, is not only the result of cellular signaling cascades. As an important organelle for cell metabolism, the integrity of mitochondrial function is also a factor that should be evaluated. Metabolite-controlled histone modifications may also be key regulators of the balance of M1-like and M2-like macrophages during stress. In addition, responses to cold stress are highly variable among species (Reynés et al., 2019; Spiljar et al., 2021). Therefore, the direct human applicability of our finding that a profound rearrangement of immune cell metabolism induced by cold exposure is associated with activation processes remains to be established.

Acknowledgments

This work was supported by the National Natural Science Foundation of China (Nos. 31672513 and 31772695), the Heilongjiang Provincial Natural Science Foundation of China (No. YQ2021C027), the Key Program of Natural Science Foundation of Heilongjiang Province (No. ZD2019C004), and the Heilongjiang Bayi Agricultural University for San Heng San Zong (No. ZRCQC202003), China.

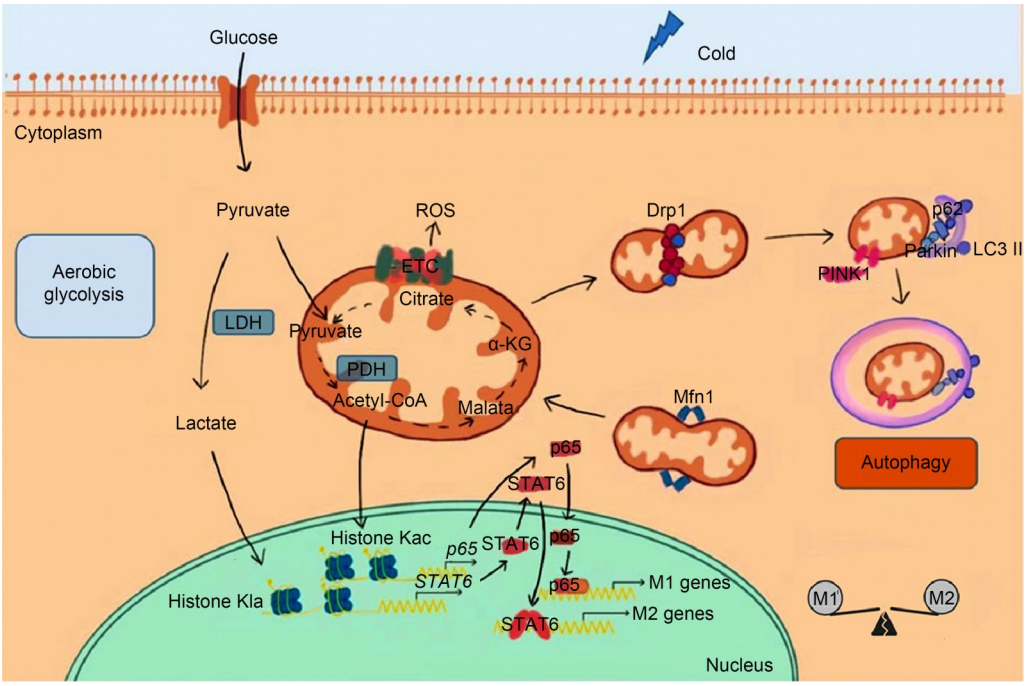

Fig. 7 Proposed model of macrophage response to cold stress. Cold stress triggers mitochondrial damage in macrophages and induces metabolic reprogramming of aerobic glycolysis. During this period, metabolic-related histone acetylation and lactylation are modulators of macrophage differentiation. ROS: reactive oxygen species; ETC: electron transport chain; PDH: pyruvate dehydrogenase; Drp1: dynamin-related protein 1; Mfn1: mitofusin 1; PINK1: PTEN-induced kinase 1; LC3: light chain 3; STAT6: signal transducer and activator of transcription 6; CoA: coenzyme A; LDH: lactate dehydrogenase; α-KG: α-ketoglutarate; Kac: acetylation; Kla: lactylation.

Author contributions

Conceptualization: Bin XU and Jingru GUO; Writing original draft, review and editing, data curation, and formal analysis: Jingjing LU and Shoupeng FU; Funding acquisition: Shize LI, Bin XU, and Huanmin YANG; Investigation: Jie DAI, Jianwen HU, Hong JI, Jiahong YU, and Jiming BAO; Methodology: Zhiquan WANG; Supervision: Bin XU and Jingru GUO.

Compliance with ethics guidelines

Jingjing LU, Shoupeng FU, Jie DAI, Jianwen HU, Shize LI, Hong JI, Zhiquan WANG, Jiahong YU, Jiming BAO, Bin XU, Jingru GUO, and Huanmin YANG declare that they have no conflict of interest.

This article does not contain any studies with human or animal subjects performed by any of the authors.

References

Amiel E, Perona-Wright G, 2020. Metabolic mediators: how immunometabolism directs the immune response to infection. *Immunology*, 161(3):163-164. https://doi.org/10.1111/imm.13275

Budhathoki NK, Zander KK, 2019. Socio-economic impact of and adaptation to extreme heat and cold of farmers in the food bowl of Nepal. *Int J Environ Res Public Health*, 16(9):1578. https://doi.org/10.3390/ijerph16091578

Castillo K, Valenzuela V, Matus S, et al., 2013. Measurement of autophagy flux in the nervous system *in vivo*. *Cell Death Dis*, 4(11):e917. https://doi.org/10.1038/cddis.2013.421

Chen YH, Liu W, Wang YW, et al., 2017. Casein Kinase 2 Interacting Protein-1 regulates M1 and M2 inflammatory macrophage polarization. *Cell Signal*, 33:107-121. https://doi.org/10.1016/j.cellsig.2017.02.015

Codo AC, Davanzo GG, de Brito Monteiro L, et al., 2020. Elevated glucose levels favor SARS-CoV-2 infection and monocyte response through a HIF-1α/glycolysis-dependent axis. *Cell Metab*, 32(3):437-446.E5. https://doi.org/10.1016/j.cmet.2020.07.007

Delavary BM, van der Veer WM, van Egmond M, et al., 2011. Macrophages in skin injury and repair. *Immunobiology*, 216(7):753-762. https://doi.org/10.1016/j.imbio.2011.01.001

Díaz J, López-Bueno JA, Sáez M, et al., 2019. Will there be cold-related mortality in Spain over the 2021–2050 and 2051–2100 time horizons despite the increase in temperatures as a consequence of climate change? *Environ Res*, 176:108557. https://doi.org/10.1016/j.envres.2019.108557

di Conza GD, Ho PC, 2018. Metabolic adaptation of macrophages in chronic diseases. *Cancer Lett*, 414:250-256. https://doi.org/10.1016/j.canlet.2017.11.023

Dumont A, Lee M, Barouillet T, et al., 2021. Mitochondria orchestrate macrophage effector functions in atherosclerosis. *Mol Aspects Med*, 77:100922. https://doi.org/10.1016/j.mam.2020.100922

Fuchs AL, Schiller SM, Keegan WJ, et al., 2019. Quantitative ^{1}H NMR metabolomics reveal distinct metabolic adaptations in human macrophages following differential activation. *Metabolites*, 9(11):248. https://doi.org/10.3390/metabo9110248

Hardbower DM, Asim M, Luis PB, et al., 2017. Ornithine decarboxylase regulates M1 macrophage activation and mucosal inflammation via histone modifications. *Proc Natl Acad Sci USA*, 114(5):E751-E760. https://doi.org/10.1073/pnas.1614958114

Horn CM, Kielian T, 2021. Crosstalk between *Staphylococcus aureus* and innate immunity: focus on immunometabolism. *Front Immunol*, 11:621750. https://doi.org/10.3389/fimmu.2020.621750

Hoshino A, Wang WJ, Wada S, et al., 2019. The ADP/ATP translocase drives mitophagy independent of nucleotide exchange. *Nature*, 575(7782):375-379. https://doi.org/10.1038/s41586-019-1667-4

Hosios AM, Vander Heiden MG, 2017. Endothelial cells get β-ox-ed in to support lymphangiogenesis. *Dev Cell*, 40(2): 118-119. https://doi.org/10.1016/j.devcel.2017.01.004

Huang CY, Kuo WW, Ho TJ, et al., 2018. Rab9-dependent autophagy is required for the IGF-IIR triggering mitophagy to eliminate damaged mitochondria. *J Cell Physiol*, 233(9): 7080-7091. https://doi.org/10.1002/jcp.26346

Iavarone F, Guardiola O, Scagliola A, et al., 2020. Cripto shapes macrophage plasticity and restricts EndMT in injured and diseased skeletal muscle. *EMBO Rep*, 21(4): e49075. https://doi.org/10.15252/embr.201949075

Indo HP, Davidson M, Yen HC, et al., 2007. Evidence of ROS generation by mitochondria in cells with impaired electron transport chain and mitochondrial DNA damage. *Mitochondrion*, 7(1-2):106-118. https://doi.org/10.1016/j.mito.2006.11.026

Jha AK, Huang SCC, Sergushichev A, et al., 2015. Network integration of parallel metabolic and transcriptional data reveals metabolic modules that regulate macrophage polarization. *Immunity*, 42(3):419-430. https://doi.org/10.1016/j.immuni.2015.02.005

Kalghatgi S, Spina CS, Costello JC, et al., 2013. Bactericidal antibiotics induce mitochondrial dysfunction and oxidative damage in mammalian cells. *Sci Transl Med*, 5(192): 192ra85. https://doi.org/10.1126/scitranslmed.3006055

Kang H, Lee Y, Bae M, et al., 2020. Astaxanthin inhibits alcohol-induced inflammation and oxidative stress in macrophages in a sirtuin 1-dependent manner. *J Nutr Biochem*, 85:108477. https://doi.org/10.1016/j.jnutbio.2020.108477

Kang SU, Kim DH, Lee YS, et al., 2021. DIM-C-pPhtBu induces lysosomal dysfunction and unfolded protein response-mediated cell death via excessive mitophagy. *Cancer Lett*, 504:23-36. https://doi.org/10.1016/j.canlet.2021.01.005

Katoh M, Wu B, Nguyen HB, et al., 2017. Polymorphic regulation of mitochondrial fission and fusion modifies phenotypes of microglia in neuroinflammation. *Sci Rep*, 7:4942. https://doi.org/10.1038/s41598-017-05232-0

Kaur S, Raggatt LJ, Batoon L, et al., 2017. Role of bone marrow macrophages in controlling homeostasis and repair in bone and bone marrow niches. *Semin Cell Dev Biol*, 61:12-21. https://doi.org/10.1016/j.semcdb.2016.08.009

Layoun A, Samba M, Santos MM, 2015. Isolation of murine peritoneal macrophages to carry out gene expression analysis upon Toll-like receptors stimulation. *J Vis Exp*, 98:e52749. https://doi.org/10.3791/52749

Li YJ, Wu YZ, Hu Y, 2021. Metabolites in the tumor microenvironment reprogram functions of immune effector cells through epigenetic modifications. *Front Immunol*, 12: 641883. https://doi.org/10.3389/fimmu.2021.641883

Lio CWJ, Huang SCC, 2020. Circles of life: linking metabolic and epigenetic cycles to immunity. *Immunology*, 161(3): 165-174. https://doi.org/10.1111/imm.13207

Lu BW, 2009. Mitochondrial dynamics and neurodegeneration. *Curr Neurol Neurosci Rep*, 9(3):212-219. https://doi.org/10.1007/s11910-009-0032-7

Ma JW, Wei KK, Liu JW, et al., 2020. Glycogen metabolism regulates macrophage-mediated acute inflammatory responses. *Nat Commun*, 11:1769. https://doi.org/10.1038/s41467-020-15636-8

MacVicar T, Ohba Y, Nolte H, et al., 2019. Lipid signalling drives proteolytic rewiring of mitochondria by YME1L. *Nature*, 575(7782):361-365. https://doi.org/10.1038/s41586-019-1738-6

Malhotra R, Tyson DGW, Sone H, et al., 2002. Glucose uptake and adenoviral mediated GLUT1 infection decrease hypoxia-induced HIF-1α levels in cardiac myocytes. *J Mol Cell Cardiol*, 34(8):1063-1073. https://doi.org/10.1006/jmcc.2002.2047

Marín Franco JL, Genoula M, Corral D, et al., 2020. Host-derived lipids from tuberculous pleurisy impair macrophage microbicidal-associated metabolic activity. *Cell Rep*, 33(13):108547. https://doi.org/10.1016/j.celrep.2020.108547

Mathew R, White E, 2011. Autophagy, stress, and cancer metabolism: what doesn't kill you makes you stronger. *Cold Spring Harb Symp Quant Biol*, 76:389-396. https://doi.org/10.1101/sqb.2012.76.011015

Matus S, Valenzuela V, Hetz C, 2014. A new method to measure autophagy flux in the nervous system. *Autophagy*, 10(4): 710-714. https://doi.org/10.4161/auto.28434

McMurtrey RJ, 2016. Analytic models of oxygen and nutrient diffusion, metabolism dynamics, and architecture

optimization in three-dimensional tissue constructs with applications and insights in cerebral organoids. *Tissue Eng Part C Methods*, 22(3):221-249. https://doi.org/10.1089/ten.TEC.2015.0375

Orecchioni M, Ghosheh Y, Pramod AB, et al., 2019. Macrophage polarization: different gene signatures in M1(LPS+) vs. classically and M2(LPS−) vs. alternatively activated macrophages. *Front Immunol*, 10:1084. https://doi.org/10.3389/fimmu.2019.01084

Palzer L, Bader JJ, Angel F, et al., 2018. Alpha-amino-beta-carboxy-muconate-semialdehyde decarboxylase controls dietary niacin requirements for NAD^+ synthesis. *Cell Rep*, 25(5):1359-1370.E4. https://doi.org/10.1016/j.celrep.2018.09.091

Reynés B, van Schothorst EM, Keijer J, et al., 2019. Effects of cold exposure revealed by global transcriptomic analysis in ferret peripheral blood mononuclear cells. *Sci Rep*, 9: 19985. https://doi.org/10.1038/s41598-019-56354-6

Rodríguez-Prados JC, Través PG, Cuenca J, et al., 2010. Substrate fate in activated macrophages: a comparison between innate, classic, and alternative activation. *J Immunol*, 185(1):605-614. https://doi.org/10.4049/jimmunol.0901698

Saggese P, Sellitto A, Martinez CA, et al., 2020. Metabolic regulation of epigenetic modifications and cell differentiation in cancer. *Cancers*, 12(12):3788. https://doi.org/10.3390/cancers12123788

Schito L, Rey S, 2018. Cell-autonomous metabolic reprogramming in hypoxia. *Trends Cell Biol*, 28(2):128-142. https://doi.org/10.1016/j.tcb.2017.10.006

Shang YL, Liu Y, Du L, et al., 2009. Targeted expression of uncoupling protein 2 to mouse liver increases the susceptibility to lipopolysaccharide/galactosamine-induced acute liver injury. *Hepatology*, 50(4):1204-1216. https://doi.org/10.1002/hep.23121

Singh K, Coburn LA, Asim M, et al., 2018. Ornithine decarboxylase in macrophages exacerbates colitis and promotes colitis-associated colon carcinogenesis by impairing M1 immune responses. *Cancer Res*, 78(15):4303-4315. https://doi.org/10.1158/0008-5472.Can-18-0116

Spiljar M, Steinbach K, Rigo D, et al., 2021. Cold exposure protects from neuroinflammation through immunologic reprogramming. *Cell Metab*, 33(11):2231-2246.E8. https://doi.org/10.1016/j.cmet.2021.10.002

Stienstra R, Netea-Maier RT, Riksen NP, et al., 2017. Specific and complex reprogramming of cellular metabolism in myeloid cells during innate immune responses. *Cell Metab*, 26(1):142-156. https://doi.org/10.1016/j.cmet.2017.06.001

Suárez-Rivero JM, Villanueva-Paz M, de la Cruz-Ojeda P, et al., 2017. Mitochondrial dynamics in mitochondrial diseases. *Diseases*, 5(1):1. https://doi.org/10.3390/diseases5010001

Sun K, Guo XL, Zhao QD, et al., 2013. Paradoxical role of autophagy in the dysplastic and tumor-forming stages of hepatocarcinoma development in rats. *Cell Death Dis*, 4(2):e501. https://doi.org/10.1038/cddis.2013.35

van den Bossche J, O'Neill LA, Menon D, 2017. Macrophage immunometabolism: where are we (going)? *Trends Immunol*, 38(6):395-406. https://doi.org/10.1016/j.it.2017.03.001

van Winkle LJ, Ryznar R, 2019. One-carbon metabolism regulates embryonic stem cell fate through epigenetic DNA and histone modifications: implications for transgenerational metabolic disorders in adults. *Front Cell Dev Biol*, 7:300. https://doi.org/10.3389/fcell.2019.00300

Wang FL, Zhang S, Jeon R, et al., 2018. Interferon gamma induces reversible metabolic reprogramming of M1 macrophages to sustain cell viability and pro-inflammatory activity. *eBioMedicine*, 30:303-316. https://doi.org/10.1016/j.ebiom.2018.02.009

Wang TT, Zhang H, Han YB, et al., 2019. Light-enhanced O_2-evolving nanoparticles boost photodynamic therapy to elicit antitumor immunity. *ACS Appl Mater Interfaces*, 11(18):16367-16379. https://doi.org/10.1021/acsami.9b03541

Wang ZJ, Long H, Chang C, et al., 2018. Crosstalk between metabolism and epigenetic modifications in autoimmune diseases: a comprehensive overview. *Cell Mol Life Sci*, 75(18):3353-3369. https://doi.org/10.1007/s00018-018-2864-2

Wang ZQ, Zhao YW, Xu NH, et al., 2019. NEAT1 regulates neuroglial cell mediating Aβ clearance via the epigenetic regulation of endocytosis-related genes expression. *Cell Mol Life Sci*, 76(15):3005-3018. https://doi.org/10.1007/s00018-019-03074-9

Xie W, Tang Q, Yan F, et al., 2021. Transcriptional memory and response to adverse temperatures in plants. *J Zhejiang Univ-Sci B (Biomed & Biotechnol)*, 22(10):791-804. https://doi.org/10.1631/jzus.B2100287

Xu B, Lian S, Li SZ, et al., 2018. GABAB receptor mediate hippocampal neuroinflammation in adolescent male and female mice after cold expose. *Brain Res Bull*, 142: 163-175. https://doi.org/10.1016/j.brainresbull.2018.07.011

Xu B, Zang SC, Li SZ, et al., 2019. HMGB1-mediated differential response on hippocampal neurotransmitter disorder and neuroinflammation in adolescent male and female mice following cold exposure. *Brain Behav Immun*, 76:223-235. https://doi.org/10.1016/j.bbi.2018.11.313

Xu C, Liu Q, Liang JJ, et al., 2021. Urinary biomarkers of polycyclic aromatic hydrocarbons and their associations with liver function in adolescents. *Environ Pollut*, 278: 116842. https://doi.org/10.1016/j.envpol.2021.116842

Yang FQ, Liu M, Yang FP, et al., 2014. VPA inhibits renal cancer cell migration by targeting HDAC2 and down-regulating HIF-1α. *Mol Biol Rep*, 41(3):1511-1518. https://doi.org/10.1007/s11033-013-2996-2

Youle RJ, van der Bliek AM, 2012. Mitochondrial fission, fusion, and stress. *Science*, 337(6098):1062-1065. https://doi.org/10.1126/science.1219855

Yu S, Du MY, Yin A, et al., 2020. Bcl-xL inhibits PINK1/Parkin-dependent mitophagy by preventing mitochondrial Parkin accumulation. *Int J Biochem Cell Biol*, 122: 105720. https://doi.org/10.1016/j.biocel.2020.105720

Yu T, Zhao L, Huang X, et al., 2016. Enhanced activity of the macrophage M1/M2 phenotypes and phenotypic switch to M1 in periodontal infection. *J Periodontol*, 87(9): 1092-1102. https://doi.org/10.1902/jop.2016.160081

Zhang D, Tang ZY, Huang H, et al., 2019. Metabolic regulation of gene expression by histone lactylation. *Nature*, 574(7779):575-580. https://doi.org/10.1038/s41586-019-1678-1

Zheng QF, Maksimovic I, Upad A, et al., 2020. Non-enzymatic covalent modifications: a new link between metabolism and epigenetics. *Protein Cell*, 11(6):401-416. https://doi.org/10.1007/s13238-020-00722-w

Zheng T, Zhan J, Yang M, et al., 2021. Hemin-induced increase in saponin content contributes to the alleviation of osmotic and cold stress damage to conyza blinii in a heme oxygenase 1-dependent manner. *J Zhejiang Univ-Sci B (Biomed & Biotechnol)*, 22(8):682-694. https://doi.org/10.1631/jzus.B2000697